

# System Parameters for the Eclipsing B-star Binary HD 42401

S. J. Williams<sup>1</sup>

*Center for High Angular Resolution Astronomy and  
Department of Physics and Astronomy,  
Georgia State University, P. O. Box 4106, Atlanta, GA 30302-4106;  
swilliams@chara.gsu.edu*

## ABSTRACT

I present results from an optical spectroscopic investigation of the binary system HD 42401 (V1388 Ori; B2.5 IV-V + B3 V). A combined analysis of  $V$ -band photometry and radial velocities indicates that the system has an orbital period of  $2.18706 \pm 0.00005$  days and an inclination of  $75.5 \pm 0.2$  degrees. This solution yields masses and radii of  $M_1 = 7.42 \pm 0.08 M_\odot$  and  $R_1 = 5.60 \pm 0.04 R_\odot$  for the primary and  $M_2 = 5.16 \pm 0.03 M_\odot$  and  $R_2 = 3.76 \pm 0.03 R_\odot$  for the secondary. Based on the position of the two stars plotted on a theoretical H-R diagram, I find that the age of the system is  $\gtrsim 25$  Myr and that both stars appear overluminous for their masses compared to single star evolutionary tracks. A fit of the spectral energy distribution based on photometry from the literature yields a distance to HD 42401 of  $832 \pm 89$  parsecs.

*Subject headings:* binaries: spectroscopic – stars: early-type – stars: fundamental parameters – stars: individual (HD 42401)

## 1. Introduction

Two fundamental parameters in stellar astrophysics are the masses and radii of stars. Especially lacking are accurate ( $\leq 2\%$ ) determinations of these quantities for O- and B-type systems. Data of this kind are important for tests of stellar models, with far-reaching implications such as the modeling of stellar components of galaxies. Here I describe measurements of these parameters for the B-star binary HD 42401. This effort is part of an

---

<sup>1</sup>Visiting Astronomer, Kitt Peak National Observatory, National Optical Astronomy Observatory, which is operated by the Association of Universities for Research in Astronomy (AURA) under cooperative agreement with the National Science Foundation.

ongoing program to determine the masses and radii of O- and B-type stars. Previously, I obtained parameters for the LMC O-star binary [L72] LH 54-425 (Williams et al. 2008) and will continue with more analyses of eclipsing spectroscopic binary systems containing O- and B-type stars.

The star HD 42401 was first classified as B2 V by Walborn (1971). Since then, it has been used as a spectral standard for the B2 V type stars in a number of publications (Walborn & Fitzpatrick 1990; de Mello et al. 2000; Bagnuolo et al. 2001). The eclipsing nature of its light curve was first noticed with the *Hipparcos* satellite (HIP 29321), where it was classified as an Algol-type eclipsing binary and given the moniker V1388 Ori (Kazarovets et al. 1999). Three radial velocity measurements of HD 42401 by Fehrenbach et al. (1997) show a range from  $-103$  to  $36$  km s $^{-1}$ , but no further investigations were made into this probable velocity variable.

Presented here are the analyses of radial velocities from optical spectra obtained in 2008 January (§2). Section 3 contains a description of the measurement of radial velocities from the data. In §4 I describe tomographic reconstructions of the individual component spectra. Covered in §5 is the combined light curve and radial velocity curve solution. In §6 I finish with a discussion of the distance to the system, its fundamental parameters, and other consequences of the analysis.

## 2. Observations

I obtained 29 spectra of HD 42401 with the Kitt Peak National Observatory (KPNO) 0.9-m coudé feed telescope during an observing run from 2008 Jan 09 to 2008 Jan 18. These spectra were obtained with the long collimator and grating A (632 grooves mm $^{-1}$  with a blaze wavelength of 6000 Å in second order with order sorting filter 4-96). The first two nights of observations were made with the T1KB detector (1024×1024 pixel array with 24 square  $\mu$ m pixels) and resulted in a resolving power of  $R = \lambda/\delta\lambda = 13,500$  with wavelength coverage from 4315–4490 Å. The rest of the observing run made use of the F3KB detector (3072×1024 pixel array with 15 square  $\mu$ m pixels) that resulted in a lower resolving power of  $R = \lambda/\delta\lambda = 11,500$  with wavelength coverage from 4250–4570 Å. The wavelength coverage was chosen to include the He I  $\lambda 4471$  and Mg II  $\lambda 4481$  lines that are good temperature indicators for B-type stars plus the H $\gamma$  line that is sensitive to gravity (linear stark effect). Exposure times were 1200 s giving a S/N  $\simeq 100$  pixel $^{-1}$ . Numerous comparison spectra were obtained for wavelength calibration, and many bias and flat field spectra were also obtained each night.

The spectra were extracted and calibrated using standard routines in IRAF<sup>2</sup>, and then each continuum rectified spectrum was transformed to a common heliocentric wavelength grid in  $\log \lambda$  increments.

### 3. Radial Velocities

The narrow range of wavelength coverage in our spectra limits the lines that may be used for radial velocity analysis. I measured radial velocities from three lines, He I  $\lambda 4387$ , He I  $\lambda 4471$ , and Mg II  $\lambda 4481$  via a template-fitting scheme (Gies et al. 2002) that measures velocities by using model templates weighted by a flux ratio to match both the shifts and line depths in the observed spectra. There is no evidence of emission or intrinsic line asymmetries in these lines or H $\gamma$   $\lambda 4340$ .

The BSTAR2006 grid of stellar models from Lanz & Hubeny (2007) was used to derive template spectra. These models are based on the line blanketed, non-LTE, plane-parallel, hydrostatic atmosphere code TLUSTY and the radiative transfer code SYNSPEC (Hubeny 1988; Hubeny & Lanz 1995; Hubeny et al. 1998). In finding templates, initial values were used for temperatures, gravities, projected rotational velocities, and flux contributions from each star. These parameters for model templates were then checked by comparing the three lines used in radial velocity measurements against the tomographically reconstructed spectra of each star (§4). The parameters were changed and new templates made after initial fits to the light curve and radial velocity curves (§5) indicated slightly different values were more appropriate. The velocity analysis was then performed again until the best fit was obtained. In this way, I was able to obtain an estimate of the monochromatic flux ratio in the blue spectra of  $F_2/F_1 = 0.25 \pm 0.05$  based upon the relative line depths of the spectral components.

The template fitting scheme also needs preliminary estimates for the velocities of each component. To obtain these, spectra which clearly showed two sets of spectral lines were analyzed. Midpoints of spectral features were used to make crude estimates of radial velocities for each star. Preliminary orbital parameters were obtained by using the nonlinear, least-squares fitting program of Morbey & Brosterhus (1974). The preliminary velocities from this initial orbital solution were starting points for performing a nonlinear, least-squares fit of the composite profiles with the template spectra and calculating the shifts for each star.

---

<sup>2</sup>IRAF is distributed by the National Optical Astronomy Observatory, which is operated by the Association of Universities for Research in Astronomy, Inc., under cooperative agreement with the National Science Foundation.

The fitting scheme searches a region of  $\pm 10 \text{ \AA}$  around the rest wavelength of each line, so preliminary velocities are mere starting points and need not be highly accurate. The three values for radial velocity from each spectrum were averaged, and the standard deviation of the mean value was calculated. Each of these values are listed in Table 1 for the primary and secondary stars. Also listed are the orbital phase for each observation and the observed minus calculated values for each data point. Phase zero is defined as the time of inferior conjunction of the primary star,  $T_{\text{IC},1}$  (time of secondary minimum in the light curve). Figure 1 shows two sample spectra at times of near quadrature according to this ephemeris.

During eclipse phases, velocity measurements may be affected by the Rossiter-McLaughlin effect in which the center of light of the eclipsed star will appear redshifted on ingress and blue shifted on egress because of the rotational Doppler shifts of the visible portions. This effect will result in narrower line profiles as the red and blue shifted regions of the eclipsed star are blocked, and it is more prominent in broad-lined, rapidly rotating systems. HD 42401 is a short period binary having relatively narrow lines, therefore the effect should be small. However, since the template method does not account for eclipses, deviations from orbital motion near eclipse phases are expected.

#### 4. Tomographic Reconstruction

The Doppler tomography algorithm of Bagnuolo et al. (1994) was used to separate the primary and secondary spectra of HD 42401 for the F3KB spectra. This iterative method uses the 24 observed composite spectra, their velocity shifts, and an assumed monochromatic flux ratio to derive individual component spectra. The best flux ratio was the one that best matched line depths in the reconstructions with those in the model spectra. Figure 2 shows the reconstructed spectra for the primary and secondary with the best fit models overplotted. The relative depths of He I  $\lambda 4471$  and Mg II  $\lambda 4481$  are good temperature indicators throughout the B-star sequence. Specifically, the He I  $\lambda 4471$  line gets weaker while the Mg II  $\lambda 4481$  line gets stronger as temperature decreases, as is seen in the spectrum of the secondary compared to that of the primary. The set of spectra from the F3KB instrument has only one spectrum that is close to an eclipse. Because there are many more spectra outside eclipse used in the tomographic reconstruction, the final reconstructed spectra are insensitive to details of the Rossiter-McLaughlin effect. Indeed, tomographic reconstructions with the one eclipse spectrum omitted are negligibly different from those presented in Fig. 2.

The final reconstructed spectra were fit with TLUSTY/SYNSPEC model synthesis spectra (see §3). Fits to all three lines made in the velocity analysis were used to estimate the

projected rotational velocity  $V \sin i$ , and the temperature and surface gravity of each star were estimated by comparing the reconstructed and model profiles for a grid of test values (details are given in Williams et al. 2008). These parameter values are listed in Table 2.

The narrow wavelength range of the spectra is insufficient to attempt classical spectral typing. However, I can arrive at an estimate of the spectral types for each star in the HD 42401 system by comparing the derived effective temperatures with a spectral type versus effective temperature relation. According to Table 2 of Böhm-Vitense (1981) the effective temperature and gravity (§5) of the primary of HD 42401 is most consistent with a B2.5 IV-V star while the secondary matches most closely with a B3 V star, and these classifications are listed in Table 2.

## 5. Combined Radial Velocity and Light Curve Solution

The All Sky Automated Survey (ASAS-3; Pojmanski 2002) database contains light curves for  $\sim 39,000$  previously unknown variable stars. I extracted the  $V$ -band light curve for HD 42401 (ASAS 061059+1159.7) from this catalog, removing points deemed lower quality by the data reduction pipeline used by the ASAS.

I used the Eclipsing Light Curve (ELC) code (Orosz & Hauschildt 2000) to find orbital and astrophysical parameters for the HD 42401 system. ELC fits the radial velocity and light curves simultaneously, giving a joint orbital ephemeris based on both sets of data. The best fit for the radial velocity curve is shown in Figure 3(upper panel) along with the observed minus calculated residuals (lower panel). ELC treats calculation of velocities during eclipse via a flux-weighted velocity centroid as described in Wilson & Sofia (1976). The Rossiter-McLaughlin effect is clearly seen in the best fit as a slight redshift going into eclipse and a slight blueshift leaving eclipse and the model velocity curves match the data well. The best fit for the  $V$ -band light curve is shown in Figure 4. Figures 5 and 6 show the details of the fit for the light curve in the region of the primary and secondary eclipses, respectively.

The genetic optimizer mode of ELC was used initially to explore wide ranges of values for the period, epoch of inferior conjunction of the primary  $T_{IC,1}$ , inclination, mass ratio, primary velocity semiamplitude, and Roche lobe filling factor for each star. The Roche lobe filling factor is defined by Orosz & Hauschildt (2000) as the ratio of the radius of the star toward the inner Lagrangian point ( $L_1$ ) to the distance to  $L_1$  from the center of the star,  $f \equiv x_{\text{point}}/x_{L1}$ .

The use of ELC included fixing the temperature of each star to the values found in the tomographic reconstructions (§4) and also fixing the radius ratio ( $R_1/R_2$ ) based upon

the temperatures, surface fluxes, and monochromatic flux ratio of the two stars. Non-zero eccentricities for the HD 42401 system were explored during fitting but rejected based on the higher  $\chi^2$  values for those fits.

To estimate the uncertainties based on our best fit, the values of the seven fitted parameters were varied in the calculation of  $\sim 3 \times 10^6$  light and radial velocity curves. The well-explored  $\chi^2$  surface was then projected as a function of each fitted parameter or astrophysical parameter of interest. The lowest  $\chi^2$  value is found for each parameter, and the  $1\text{-}\sigma$  uncertainty may be estimated by the region where  $\chi^2 \leq \chi_{\text{min}}^2 + 1$ . These values and uncertainties are listed in Table 3 for the orbital parameters and Table 4 for the astrophysical parameters. Also listed are  $R_{\text{eff}}$ , the effective radius of a sphere with the same volume,  $R_{\text{pole}}$ , the polar radius of each star, and  $R_{\text{point}}$ , the radius of the each star toward the inner Lagrangian point. Our derived period of  $P = 2.18706 \pm 0.00005$  days for HD 42401 agrees well with the value found by the *Hipparcos* satellite of  $2.18709 \pm 0.00050$  days (ESA 1997).

## 6. Discussion and Conclusions

The goal with this work was to determine the masses and radii of the stars in the HD 42401 system to great accuracy. I have determined the masses of the two stars to 1.1% and 0.6% and the radii of the stars to 0.7% and 0.8%, for the primary and secondary respectively. Armed with these numbers and the results from Table 4, I can consider the details of the HD 42401 system.

As is seen in Table 4, both stars are well within their Roche radii but experience tidal distortion that is evident in the light curve (Fig. 4). The rotational velocities derived from the tomographic reconstructions (Table 2) match very well with the synchronous rotation values found by ELC (Table 4), indicating that this system has achieved synchronous rotation, and is therefore not very young.

To make an estimate of the age of the system, I used the effective temperatures from Table 2 and radii from Table 4 to plot the two stars of HD 42401 on a theoretical H-R diagram and compare their locations to evolutionary tracks. The result is shown in Figure 7, plotted against evolutionary tracks for stars of 5, 7, and 9  $M_{\odot}$  from Schaller et al. (1992) as well as isochrones from Lejeune & Schaerer (2001) for solar metallicity with ages of 21.9, 25.1, 27.5, and 31.6 Myr. The location of the stars is most consistent with an age of  $\sim 25$  Myr. The model tracks shown in Figure 7 are for non-rotating stellar models. The present ratios of spin angular velocity to critical angular velocity are  $\Omega/\Omega_{\text{crit}} = 0.45$  and 0.31 for the primary and secondary, respectively (assuming synchronous rotation), and the evolutionary tracks

for such moderate rotation rates are only slightly steeper and more extended in time than those illustrated (Ekström et al. 2008). Thus, our derived age may slightly underestimate the actual value.

Both stars appear (in Fig. 7) to be overluminous for the derived masses of  $7.42 M_{\odot}$  for the primary and  $5.16 M_{\odot}$  for the secondary. Table 3 of Harmanec (1988) lists astrophysical parameters for stars as a function of spectral type for main sequence stars based on empirical data from eclipsing binaries. The mass and effective temperature of the primary fit between the listed values for spectral types B2 (mean of  $8.6 M_{\odot}$ ) and B3 (mean of  $6.1 M_{\odot}$ ), but the radius is much larger than the means for comparable spectral types and matches a B0.5 star (mean of  $5.5 R_{\odot}$ ). The mass of the secondary is consistent with the B4 spectral type (mean of  $5.1 M_{\odot}$ ) while the effective temperature and radius appear more consistent with the B3 spectral type. In a study of eclipsing binaries in the Small Magellanic Cloud, Hilditch et al. (2005) found several systems of comparable mass that, like HD 42401, are overluminous compared to model predictions. However, our findings for HD 42401 seem to conflict with the results of Malkov (2003) who shows that early B-type stars that are in close systems and rotate more slowly than single stars are on average smaller than those same single stars. In a subsequent paper, Malkov (2007) studied well-separated binaries in an effort to use the properties of their component stars for a more direct comparison with single stars. His resulting mass-luminosity-radius relations, when applied to our results for HD 42401, predict less luminous, hotter and smaller components. This is perhaps not surprising, due to the age of HD 42401 and the evolution of its components from the zero age main sequence.

I can also estimate the distance to the system by fitting a spectral energy distribution (SED) to various photometric measurements. The spectra were not flux calibrated, so to create an SED, I must rely on photometry performed on the system. HD 42401 is a relatively bright ( $V \sim 7.4$ ) system and has thus been well studied. The problem arises in estimating the phase at which a particular observation in the historical literature was made. Two observations of HD 42401 were taken by *IUE* at  $\phi = 0.12 \pm 0.07$  based on our orbital ephemeris. The uncertainty in this estimate comes from the uncertainties in our values for  $T_{\text{IC},1}$  and period and the number of orbits between the *IUE* observations and our observations. The range in uncertainty for the orbital phase of the *IUE* data brings it close to eclipse, and this was supported by initial SED fits including the *IUE* data that indicated a lower UV flux than indicated by other measurements. There are various other measurements that also were sufficiently close to eclipses to be omitted in SED fitting. Fortunately, 2MASS (Cutri et al. 2003) measurements were obtained at  $\phi = 0.16 \pm 0.03$  and are therefore far enough away from eclipse, within uncertainties, to be used. The only other points used were Johnson *UBV* magnitudes. To obtain these values, I used the value at quadrature from our light curve of  $V = 7.40$  and applied colors of  $(B - V) = -0.042$  and  $(U - B) = -0.620$  which are averages

of several observations that are listed by Mermilliod & Mermilliod (1994). The SED fit is shown in Figure 8 along with the  $U, B, V, J, H, K_s$  magnitudes. I used two model spectra from Lanz & Hubeny (2007) matching our values in Table 2 for the effective temperatures and gravities of each star, and scaled in the blue by the flux ratio of  $0.25 \pm 0.05$  found from the tomographic reconstructions. This fit of the SED results in a limb darkened, angular diameter for the primary of  $\theta_{\text{LD}} = 62.7 \pm 1.1 \mu\text{as}$  with a reddening of  $E(B - V) = 0.15 \pm 0.01$  mag and a ratio of total-to-selective extinction of  $R = 3.24 \pm 0.10$ . By directly comparing this angular diameter with the value for the radius of the primary, I estimate the distance of the system to be  $d = 832 \pm 89$  pc. This distance and reddening are in excellent agreement with the values in Bowen et al. (2008) of  $E(B - V) = 0.15 \pm 0.02$  mag and  $d = 0.8$  kpc.

HD 42401 has Galactic coordinates of  $\ell = 197^\circ 64$  and  $b = -3^\circ 33$  (Reed 2005). This is close to the Galactic open cluster NGC 2169 at  $\ell = 195^\circ 61$  and  $b = -2^\circ 93$  (separation  $\sim 2^\circ 07$ ). Abt (1977) found that the earliest spectral type of the cluster members of NGC 2169 was B2 III. Jeffries et al. (2007) find a reddening value of  $E(B - V) = 0.20 \pm 0.01$  mag and a distance of  $\sim 1060$  pc to NGC 2169. Proper motions for the objects are similar as well, with HD 42401 having  $\mu_\alpha \cos \delta = -2.25 \pm 1.41$  mas yr $^{-1}$  and  $\mu_\delta = -2.71 \pm 0.53$  mas yr $^{-1}$  (ESA 1997) and NGC 2169 having  $\mu_\alpha \cos \delta = -2.17 \pm 1.41$  mas yr $^{-1}$  and  $\mu_\delta = -2.52 \pm 0.53$  mas yr $^{-1}$  (Kharchenko et al. 2005). The systemic velocity derived here for HD 42401 is  $\sim 14$  km s $^{-1}$  and the average of 8 stars in NGC 2169 is 22 km s $^{-1}$  (Kharchenko et al. 2005). While the proximity of HD 42401 to NGC 2169 is intriguing and the fact that the earliest star has a similar spectral type to the components of HD 42401, actual cluster membership is unlikely. The age of NGC 2169 in the literature ranges from  $9 \pm 2$  Myr (Jeffries et al. 2007) to 7.8 Myr (Kharchenko et al. 2005), too young to comfortably fit with the data for the components of HD 42401 in Figure 7. Kharchenko et al. (2005) determined the corona radius of NGC 2169 by matching stellar densities of the cluster to that of the background and found an angular size of 0.15 degrees. The distance on the sky of HD 42401 from NGC 2169 is about 14 times this radius. The difference in distances to the two objects and their separation on the sky make cluster membership even more unlikely. However, it is possible that a wave of star formation associated with the Orion arm of the Galaxy swept through the region, leaving HD 42401 behind as it moved on and eventually led to the creation of NGC 2169.

I would like to thank the anonymous referee whose comments improved the paper. I would also like to thank Daryl Willmarth and the staff of KPNO for their assistance in making these observations possible and Jerry Orosz for clarifying some of the finer points of ELC’s calculations. I am also greatly indebted to D. R. Gies for his suggestions that improved the quality of this paper. This material is based on work supported by the National Science Foundation under grants AST 05-06573 and AST 06-06861. I gratefully acknowledge support

from the GSU College of Arts and Sciences and from the Research Program Enhancement fund of the Board of Regents of the University System of Georgia, administered through the GSU Office of the Vice President for Research. This research has made use of the SIMBAD database, operated at CDS, Strasbourg, France and of the WEBDA database, operated at the Institute for Astronomy of the University of Vienna.

## REFERENCES

- Abt, H. A. 1977, *PASP*, 89, 646
- Bagnuolo, W. G., Jr., Gies, D. R., Hahula, M. E., Wiemker, R., & Wiggs, M. S. 1994, *ApJ*, 423, 446
- Bagnuolo, W. G., Jr., Riddle, R. L., Gies, D. R., & Barry, D. J. 2001, *ApJ*, 554, 362
- Boehm-Vitense, E. 1981, *ARA&A*, 19, 295
- Bowen, D. V., et al. 2008, *ApJS*, 176, 59
- Cohen, M., Wheaton, W. A., & Megeath, S. T. 2003, *AJ*, 126, 1090
- Cutri, R. M., et al. 2003, *The 2MASS All-Sky Point Source Catalog of Point Sources* (Pasadena: IPAC/Caltech)
- de Mello, D. F., Leitherer, C., & Heckman, T. M. 2000, *ApJ*, 530, 251
- Ekström, S., Meynet, G., Maeder, A., & Barblan, F. 2008, *A&A*, 478, 467
- ESA 1997, *The Hipparcos and Tycho Catalogues* (ESA SP-1200)(Noordwijk: ESA)
- Fehrenbach, C., Duflot, M., Mannone, C., Burnage, R., & Genty, V. 1997, *A&AS*, 124, 255
- Gies, D. R., Penny, L. R., Mayer, P., Drechsel, H., & Lorenz, R. 2002, *ApJ*, 574, 957
- Harmanec, P. 1988, *Bull. Astron. Inst. Cz.*, 39, 329
- Hilditch, R. W., Howarth, I. D., & Harries, T. J. 2005, *MNRAS*, 357, 304
- Hubeny, I. 1988, *Computer Physics Communications*, 52, 103
- Hubeny, I., Heap, S. R., & Lanz, T. 1998, in *Boulder Munich II: Properties of Hot Luminous Stars* (ASP Conf. Ser. Vol. 131) ed. I. D. Howarth (San Francisco: ASP), 108
- Hubeny, I., & Lanz, T. 1995, *ApJ*, 439, 875

- Jeffries, R. D., Oliveira, J. M., Naylor, T., Mayne, N. J., & Littlefair, S. P. 2007, MNRAS, 376, 580
- Kazarovets, E. V., Samus, N. N., Durlevich, O. V., Frolov, M. S., Antipin, S. V., Kireeva, N. N., & Pastukhova, E. N. 1999, IBVS, 4659
- Kharchenko, N. V., Piskunov, A. E., Röser, S., Schilbach, E., & Scholz, R.-D. 2005, A&A, 438, 1163
- Lanz, T., & Hubeny, I. 2007, ApJS, 169, 83
- Lejeune, T., & Schaerer, D. 2001, A&A, 366, 538
- Malkov, O. Y. 2003, A&A, 402, 1055
- Malkov, O. Y. 2007, MNRAS, 382, 1073
- Mermilliod, J.-C., & Mermilliod, M. 1994, Catalogue of Mean UBV Data on Stars (New York: Springer)
- Morbey, C. L., & Brosterhus, E. B. 1974, PASP, 86, 455
- Orosz, J. A., & Hauschildt, P. H. 2000, A&A, 364, 265
- Reed, B. C. 2005, AJ, 130, 1652
- Pojmanski, G. 2002, Acta Astron., 52, 397
- Schaller, G., Schaerer, D., Meynet, G., & Maeder, A. 1992, A&AS, 96, 269
- Walborn, N. R. 1971, ApJS, 23, 257
- Walborn, N. R., & Fitzpatrick, E. L. 1990, PASP, 102, 379
- Williams, S. J., et al. 2008, ApJ, 682, 492
- Wilson, R. E., & Sofia, S. 1976, ApJ, 203, 182

Table 1. HD 42401 Radial Velocity Measurements

Date (HJD–2,400,000)	Orbital Phase	$V_1$ (km s <sup>-1</sup> )	$\sigma_1$ (km s <sup>-1</sup> )	$(O - C)_1$ (km s <sup>-1</sup> )	$V_2$ (km s <sup>-1</sup> )	$\sigma_2$ (km s <sup>-1</sup> )	$(O - C)_2$ (km s <sup>-1</sup> )
54474.738	0.548	-36.3	5.4	6.9	90.6	3.8	12.9
54474.836	0.593	-71.7	3.3	-1.3	138.1	13.8	4.9
54476.690	0.441	82.7	0.4	2.3	-45.7	6.3	20.4
54476.735	0.461	65.6	3.3	-1.6	-21.1	8.3	18.1
54476.775	0.480	53.8	1.6	5.7	-35.8	21.7	-20.9
54477.672	0.890	-84.6	1.8	-3.8	152.6	6.9	1.2
54477.720	0.912	-70.4	4.0	-6.5	129.4	4.7	2.4
54477.800	0.949	-41.4	3.0	-8.9	84.4	2.0	-13.8
54478.660	0.342	139.3	0.9	-3.9	-160.9	5.4	8.2
54478.676	0.349	133.3	2.0	-6.3	-160.1	5.6	3.6
54478.718	0.368	125.0	1.9	-3.3	-156.2	5.4	-9.2
54478.779	0.396	109.6	4.1	0.3	-114.4	11.0	4.9
54478.840	0.424	87.6	2.0	-1.6	-76.1	16.9	10.9
54479.667	0.802	-128.4	0.9	-1.9	218.7	4.6	0.6
54479.718	0.825	-115.9	1.2	2.3	214.2	5.3	8.3
54479.760	0.845	-109.8	0.9	-0.8	194.8	2.0	2.4
54479.825	0.874	-90.2	0.5	1.3	174.5	2.6	7.5
54480.635	0.245	163.8	0.7	-1.5	-197.1	6.8	6.6
54480.684	0.267	163.2	3.8	-1.6	-196.5	5.7	6.2
54480.755	0.300	155.8	2.3	-3.3	-194.5	4.2	-1.0
54480.802	0.321	151.8	2.0	-0.5	-186.8	4.3	-3.9
54481.635	0.702	-127.3	2.5	1.6	240.8	6.7	20.8
54481.680	0.722	-135.7	2.4	-2.7	226.5	6.5	0.0
54481.728	0.744	-135.8	0.6	-1.1	222.2	2.5	-7.4
54481.794	0.775	-135.3	2.7	-2.5	234.0	4.6	6.9
54483.646	0.622	-94.4	2.2	-3.3	171.4	5.9	8.2
54483.687	0.640	-108.5	1.9	-5.8	180.2	2.5	-0.1
54483.757	0.672	-120.3	2.0	-1.5	200.8	2.9	-3.6
54483.839	0.710	-129.4	2.0	1.3	223.4	3.6	0.5

Table 2. Tomographic Spectral Reconstruction Parameters

Parameter	Primary	Secondary
Spectral Type...	B2.5 IV-V <sup>a</sup>	B3 V <sup>a</sup>
$T_{\text{eff}}$ (kK).....	$20.5 \pm 0.5$	$18.5 \pm 0.5$
$\log g$ (cgs).....	$3.75 \pm 0.25$	$4.00 \pm 0.25$
$V \sin i$ (km s <sup>-1</sup> )	$125 \pm 10$	$75 \pm 15$
$F_2/F_1$ (blue)	$0.25 \pm 0.05$	

<sup>a</sup>These spectral types are estimated from derived values of  $T_{\text{eff}}$  and  $\log g$ .

Table 3. Circular Orbital Solution for HD 42401

Element	Value
$P$ (days) .....	$2.18706 \pm 0.00005$
$T_{\text{IC},1}$ (HJD–2,400,000) ...	$54477.9130 \pm 0.0002$
$K_1$ (km s <sup>-1</sup> ) .....	$151.4 \pm 0.3$
$K_2$ (km s <sup>-1</sup> ) .....	$217.9 \pm 1.0$
$\gamma_1$ (km s <sup>-1</sup> ) .....	$15.32 \pm 0.07$
$\gamma_2$ (km s <sup>-1</sup> ) .....	$12.9 \pm 0.2$
rms (primary) (km s <sup>-1</sup> ) .	3.7
rms (secondary) (km s <sup>-1</sup> )	9.7
rms (photometry) (mag) .	0.007

Table 4. ELC Model Parameters for HD 42401

Parameter	Primary	Secondary
Inclination (deg) ...	$75.5 \pm 0.2$	
$M$ ( $M_{\odot}$ ) .....	$7.42 \pm 0.08$	$5.16 \pm 0.03$
$R_{\text{eff}}$ ( $R_{\odot}$ ) .....	$5.60 \pm 0.04$	$3.76 \pm 0.03$
$R_{\text{pole}}^{\text{a}}$ ( $R_{\odot}$ ) .....	$5.40 \pm 0.02$	$3.70 \pm 0.01$
$R_{\text{point}}^{\text{b}}$ ( $R_{\odot}$ ) .....	$5.97 \pm 0.02$	$3.87 \pm 0.01$
$V_{\text{sync}} \sin i$ (km s <sup>-1</sup> )	$125.5 \pm 0.9$	$84.3 \pm 0.6$
$\log g$ (cgs) .....	$3.812 \pm 0.005$	$3.999 \pm 0.006$
Filling factor .....	$0.674 \pm 0.005$	$0.588 \pm 0.010$
$a_{\text{tot}}$ ( $R_{\odot}$ ) .....	$16.48 \pm 0.05$	
$F_2/F_1$ (blue) .....	$0.27 \pm 0.04$	

<sup>a</sup>Polar radius.

<sup>b</sup>Radius toward the inner Lagrangian point.

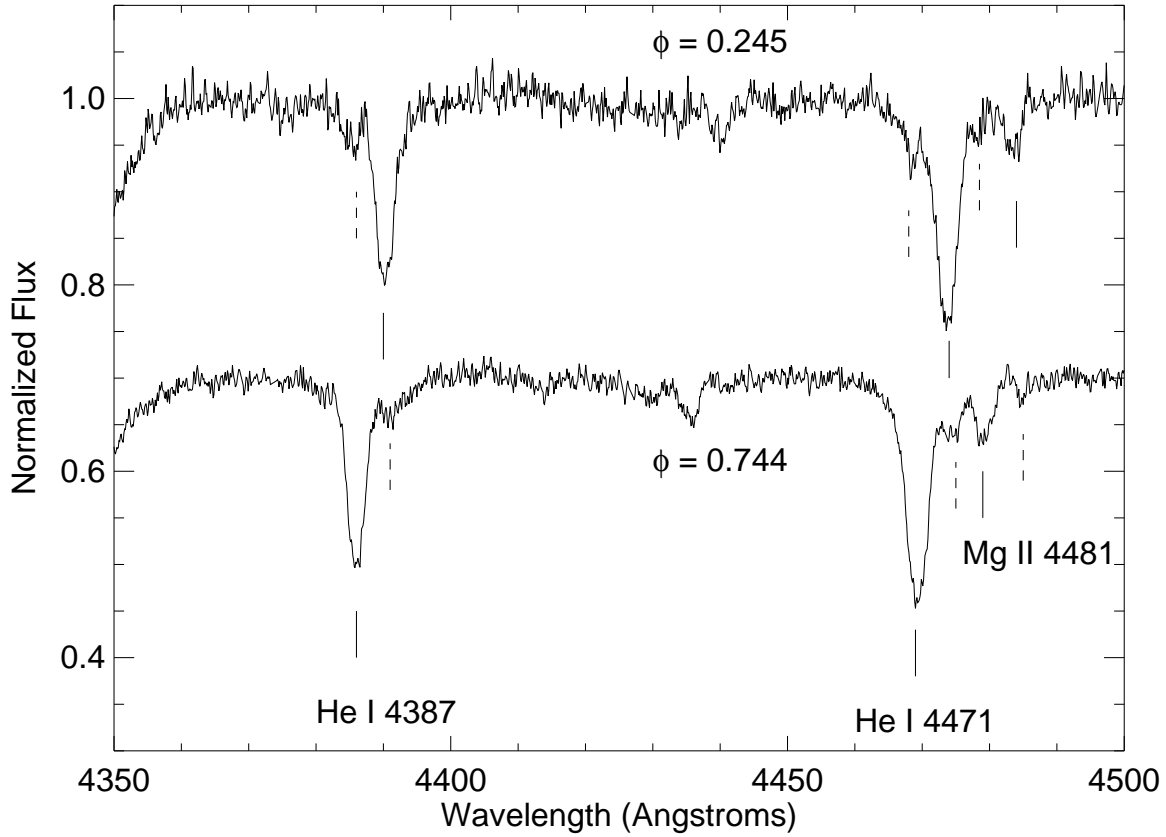


Fig. 1.— Two spectra of HD 42401 obtained near quadrature phases (offset for clarity). Solid lines indicate the positions of lines of the primary component and dashed lines indicate those for the secondary component. The lines marked are those used in the velocity analysis.

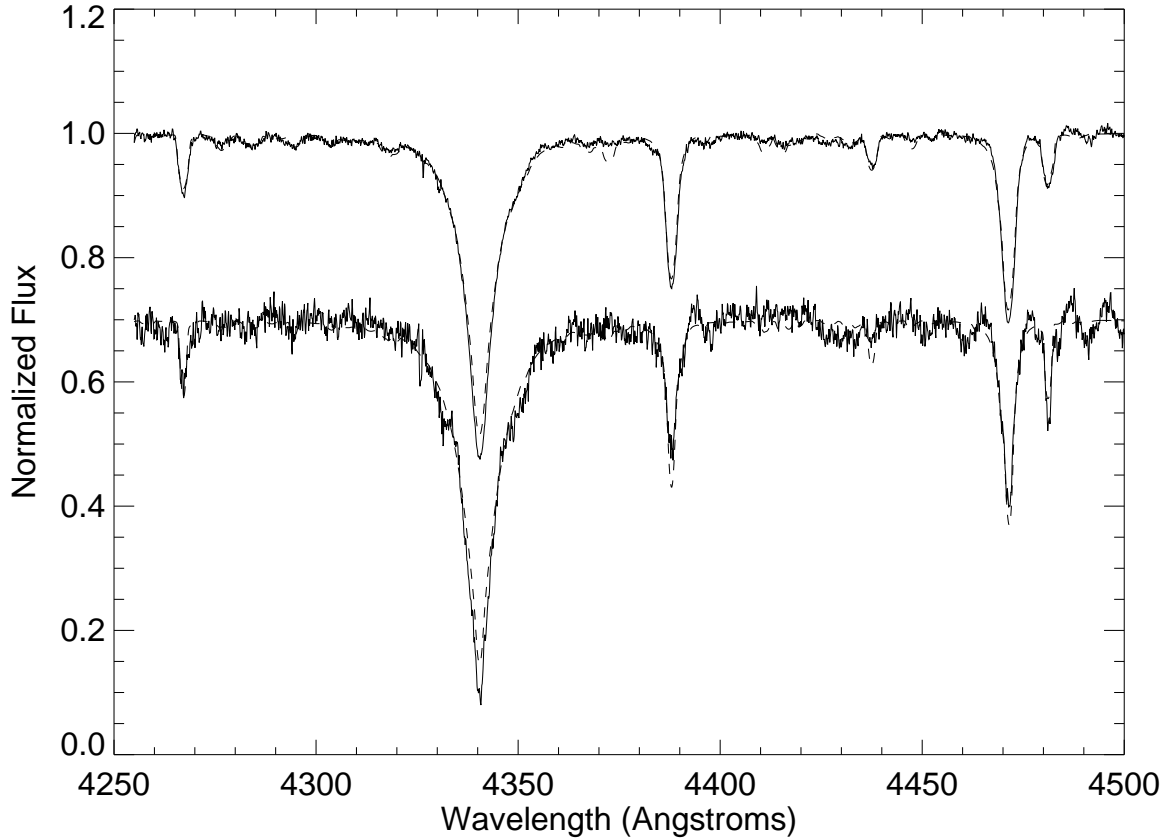


Fig. 2.— Tomographic reconstructions of the components of HD 42401 based on 24 spectra obtained with the F3KB instrument during January 2008 at KPNO. The top solid line represents the reconstructed spectrum of the primary, the bottom solid line is the reconstructed secondary spectrum offset by 0.3 for clarity. Over-plotted for both are the model spectra for each (dashed lines). The stellar parameters for the model spectra are given in Table 2.

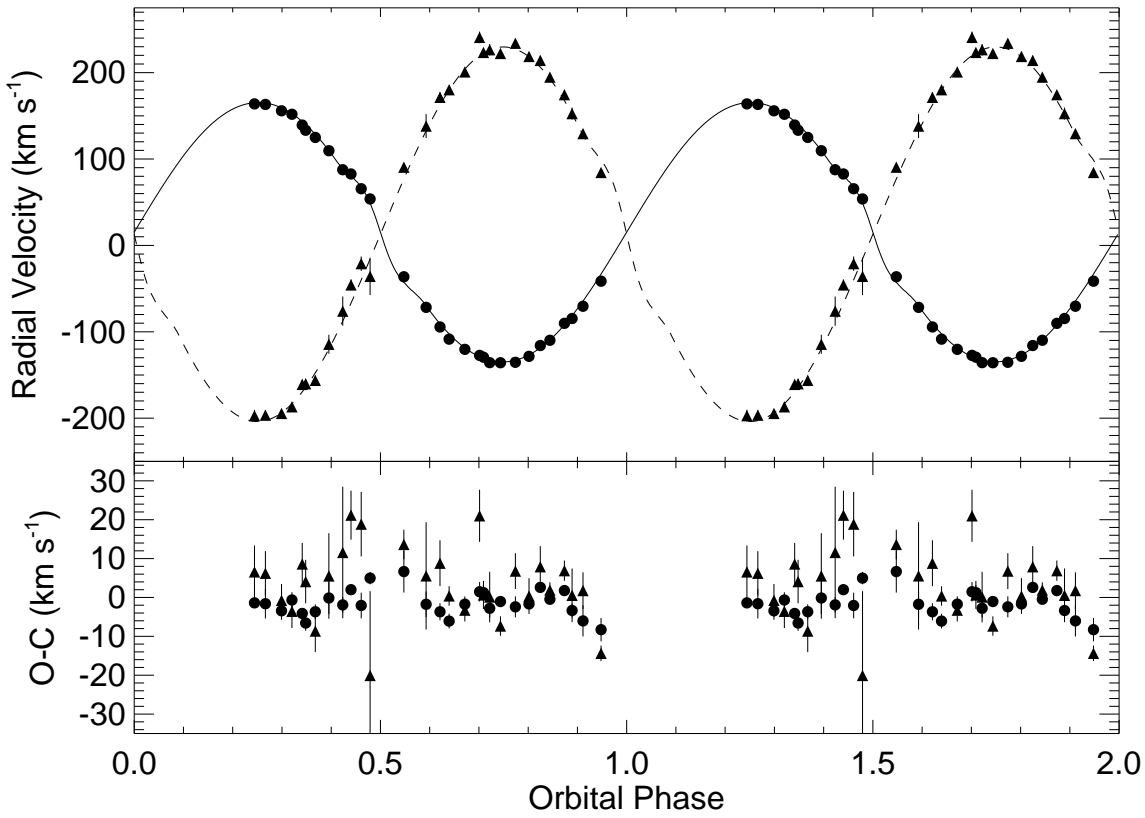


Fig. 3.— Radial velocity curves for HD 42401. Primary radial velocities are shown by filled dots and secondary radial velocities are shown by filled triangles with associated uncertainties shown as line segments for both. The solid line is the best fit solution for the primary and the dashed line is the same for the secondary. The lower panel shows the observed minus calculated values for each measurement with uncertainties.

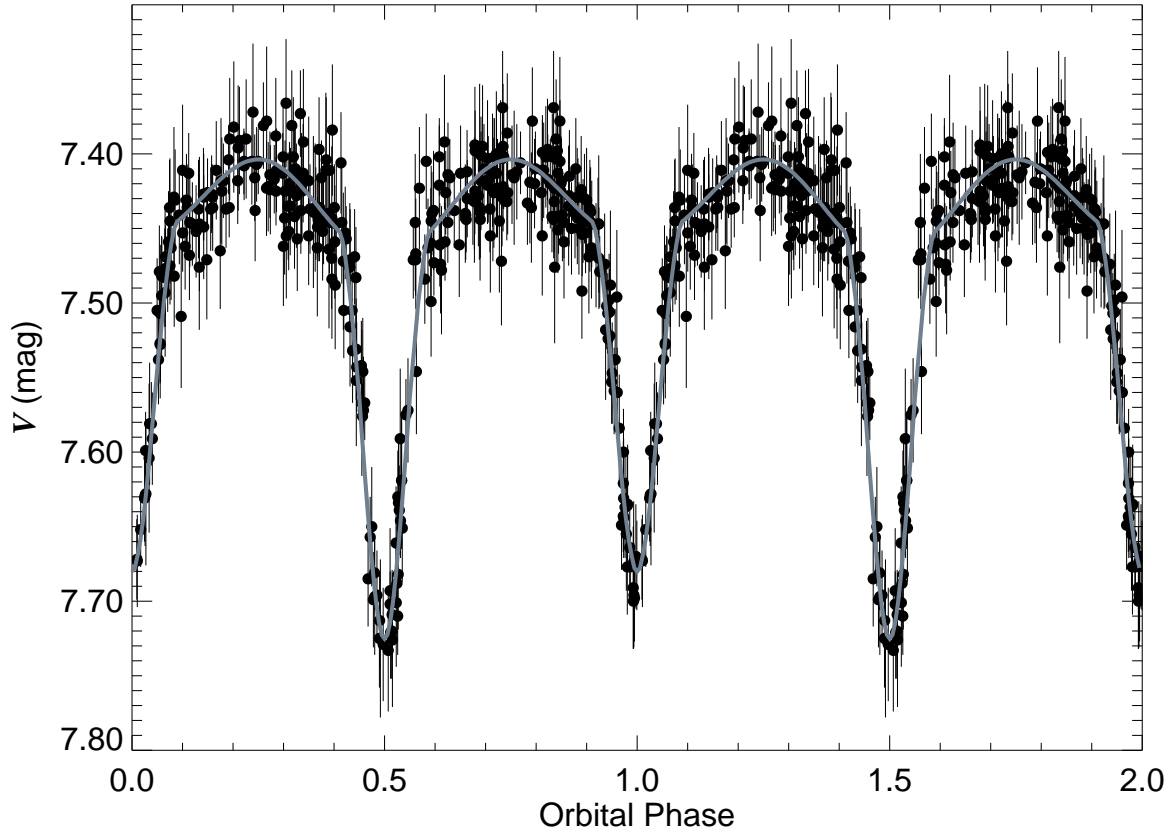


Fig. 4.—  $V$ -band light curve for HD 42401. These data were taken from the All Sky Automated Survey database (Pojmanski 2002) and are presented here in phase according to our best fit solution. The model is the thick gray line and the data are the filled dots with  $V$  uncertainties represented by line segments. Phase zero corresponds to inferior conjunction of the primary star.

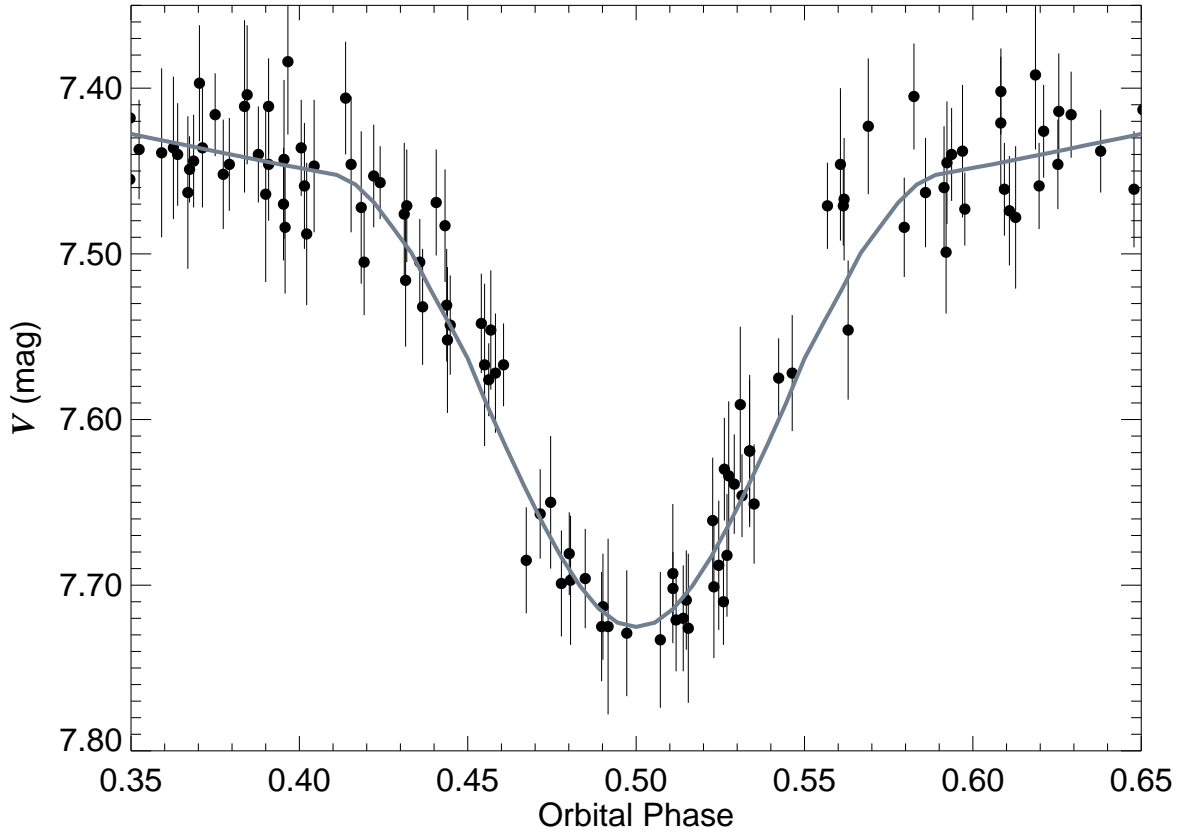


Fig. 5.—  $V$ -band light curve for HD 42401 around the time of primary eclipse. As with Fig. 4, the model is the thick gray line and the data are filled dots with line segments representing uncertainties. Residuals are distributed as expected around the best fit.

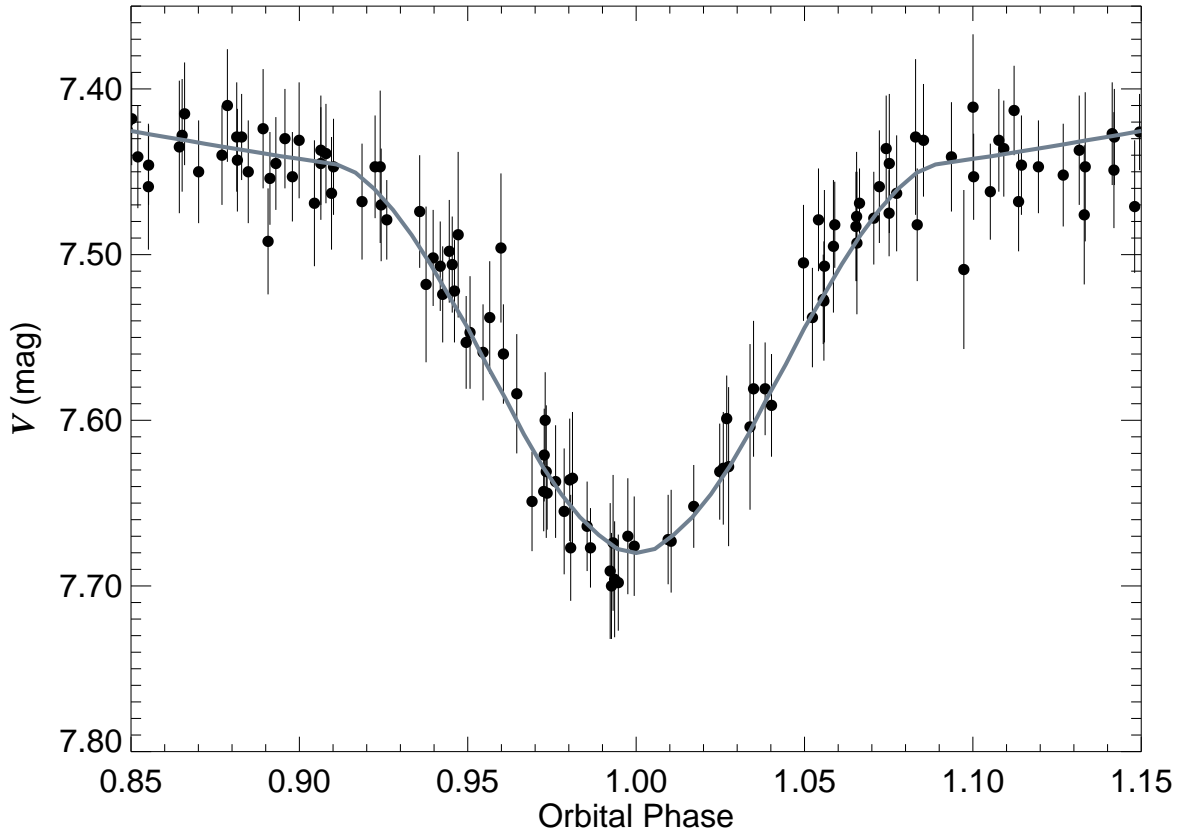


Fig. 6.—  $V$ -band light curve for HD 42401 around the time of secondary eclipse. As with Fig. 4, the model is the thick gray line and the data are filled dots with line segments representing uncertainties. Here, as in Fig. 5, the residuals are distributed as expected around the best fit.

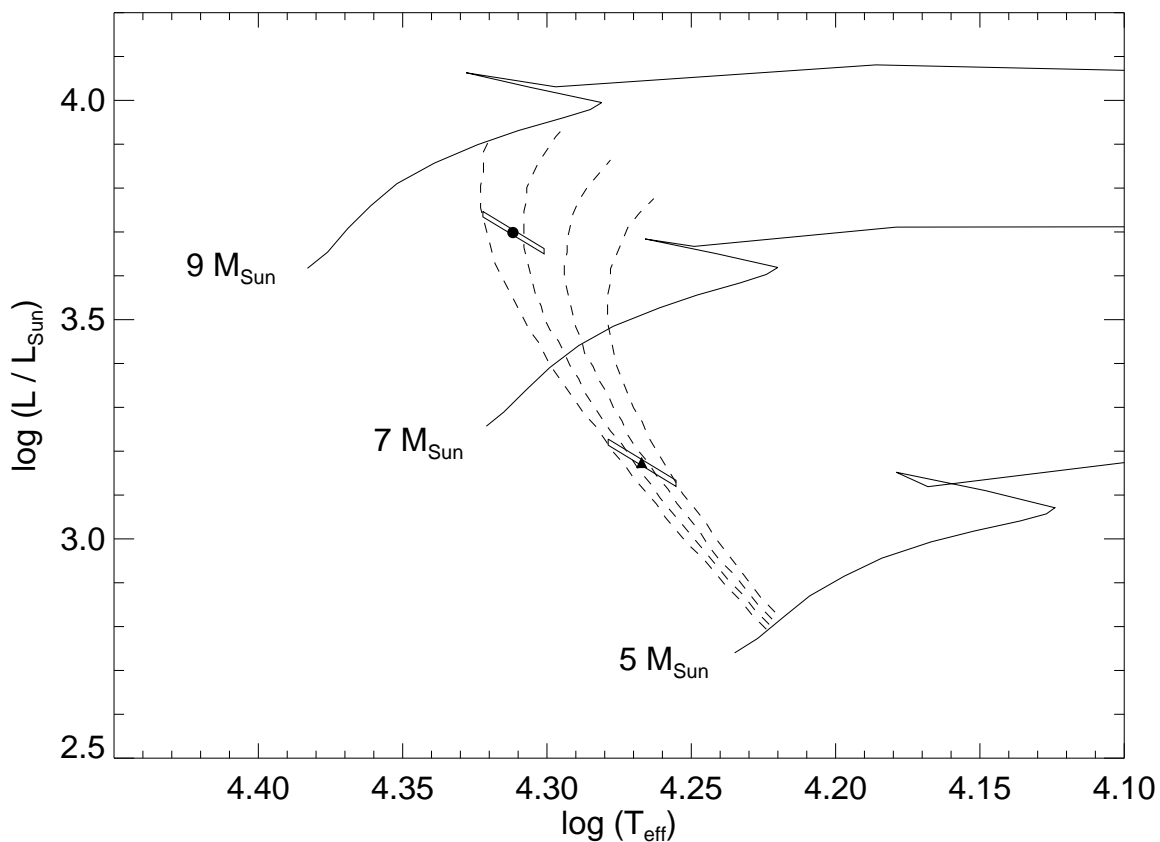


Fig. 7.— A theoretical H-R diagram showing the location of the primary star (*filled circle*) and secondary star (*filled triangle*) of HD 42401 including uncertainty regions for each. Also plotted are evolutionary tracks for stars of various masses from Schaller et al. (1992) and isochrones (*vertical dashed lines*) from Lejeune & Schaerer (2001) for solar metallicity with ages of 21.9, 25.1, 27.5, and 31.6 Myr going from left to right. The positions of the two stars are consistent with an age of  $\sim 25$  Myr.

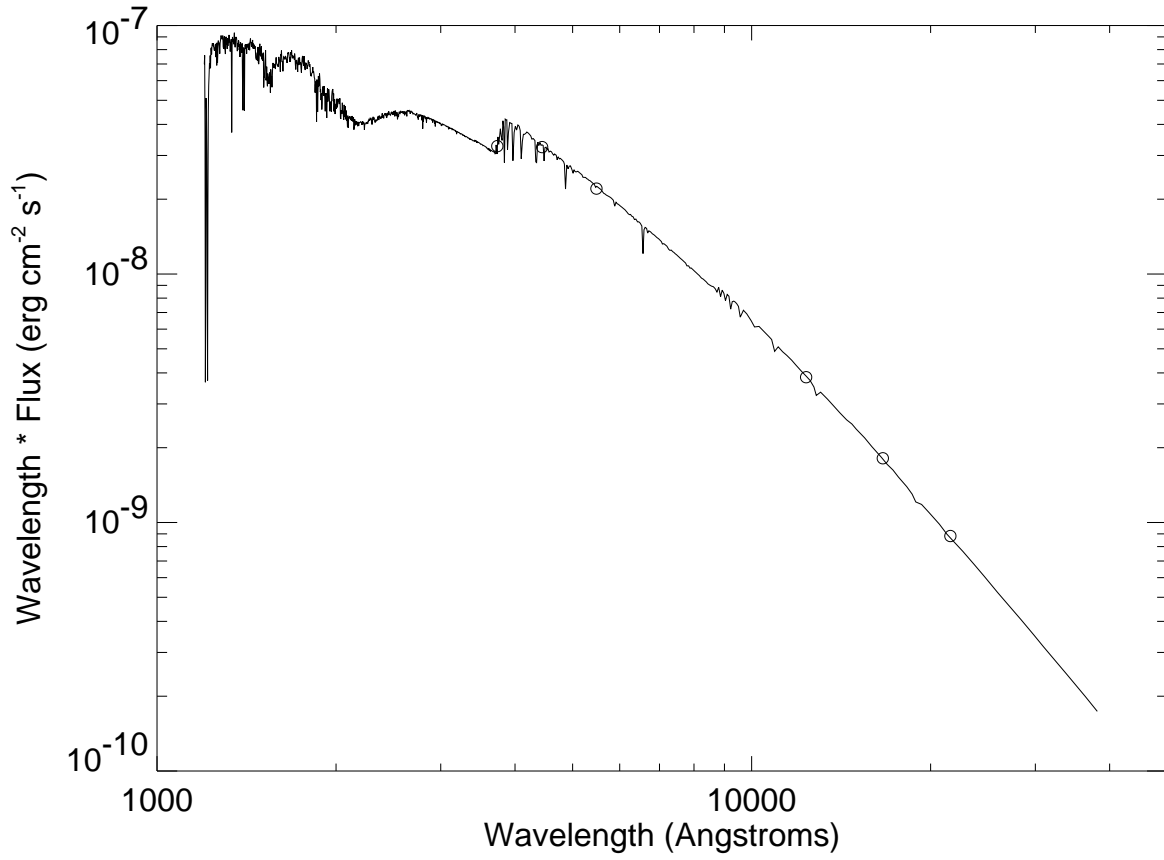


Fig. 8.— The spectral energy distribution and fit for the combined light of the HD 42401 components (*solid line*) to Johnson *U, B, V, J, H, K<sub>s</sub>* photometry (*open circles*).